

DeepIcon: A Hierarchical Network for Layer-wise Icon Vectorization

Qi Bing, Chaoyi Zhang, and Weidong Cai

School of Computer Science

The University of Sydney

NSW 2006, Australia

qbin4920@uni.sydney.edu.au, chaoyivision@gmail.com, tom.cai@sydney.edu.au

Abstract—In contrast to the well-established technique of rasterization, vectorization of images poses a significant challenge in the field of computer graphics. Recent learning-based methods for converting raster images to vector formats frequently suffer from incomplete shapes, redundant path prediction, and a lack of accuracy in preserving the semantics of the original content. These shortcomings severely hinder the utility of these methods for further editing and manipulation of images. To address these challenges, we present DeepIcon, a novel hierarchical image vectorization network specifically tailored for generating variable-length icon vector graphics based on the raster image input. Our experimental results indicate that DeepIcon can efficiently produce Scalable Vector Graphics (SVGs) directly from raster images, bypassing the need for a differentiable rasterizer while also demonstrating a profound understanding of the image contents.

Index Terms—SVG, image vectorization, vector graphics

I. INTRODUCTION

Recent research in the field of computer graphics has predominantly focused on data processing and the interpretation of raster images. In contrast, vector graphics have attracted relatively less attention within the deep learning community. Despite this, vector graphics have emerged as a preferred format across various domains, including web graphics, user interfaces, animation, and icon design, owing to their adaptability in web applications and superior scalability. Unlike raster graphics, vector graphics offer enhanced precision in

shape representation at varying resolutions and encapsulated higher-level information, such as the number of segments, sizes of segments, and the spatial relationships among paths. This inherent complexity provides significant advantages over raster graphics in many applications but poses considerable challenges for learning-based methods regarding representation, comprehension, and generation of vector graphics. In this paper, we concentrate on Scalable Vector Graphics (SVG), one of the most popular and widely utilized vector graphics formats, to explore the generation of vector graphics from images.

Image rasterization is a relatively straightforward process, whereas reversing an image to its vector representation presents significant challenges, primarily due to the potential non-uniqueness of results. Also, traditional methods perform poorly in accurately interpreting and preserving the semantics and topological characteristics of image content. In contrast, learning-based approaches have emerged as more promising in recent research, offering solutions to prevailing issues. Nevertheless, despite the advancements made by these novel approaches to image vectorization, they frequently encounter three significant obstacles: incomplete shape prediction as shown in Fig. 1c, redundant shape predictions as shown in Fig. 1a, and the inherent limitation of using pixel loss as a metric to evaluate the performance of vector graphics gener-

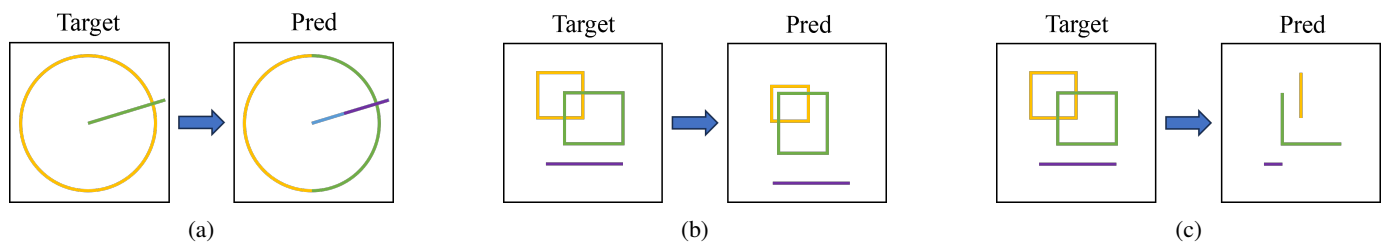


Fig. 1: Three examples of frequently encountered issues in image vectorization. The colors in the images are used to distinguish individual SVG paths. (a): An example of redundant path predictions. Despite the redundancy, the rendered output remains quantitatively accurate, indicating that redundant paths may not be reflected through the evaluation metrics. (b): In this case, the prediction performance results in low quantitative accuracy due to the geometric offset of the predicted paths. However, this example demonstrates the model’s capability to grasp the underlying semantics and relationships between shapes, such as recognizing two rectangles and one line. (c): Compared with (b), predicting shapes incompletely but with accurate positioning may achieve higher pixel accuracy.

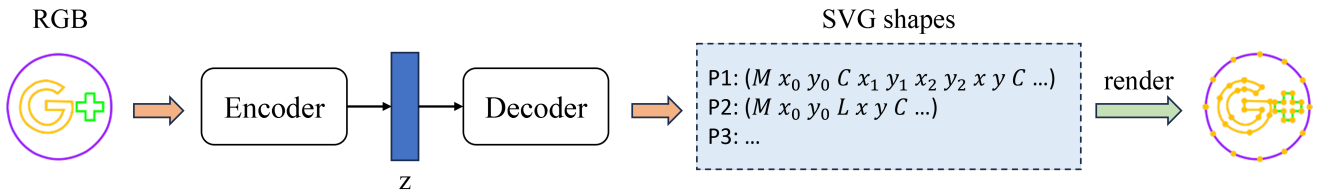


Fig. 2: The fundamental workflow that DeepIcon performs image vectorization, converting images into SVG format. Initially, the image undergoes encoding to transform into a single embedding. This embedding is then fed into a decoder to generate a sequence of parametric shapes.

ation as shown in Fig. 1b. Low processing speed can make vectorization impractical for real-time applications or large-scale processing tasks. On the other hand, unnecessary complexity in layer segmentation can result in vectorized images that are difficult to edit or manipulate, limiting their utility for graphic design and professional artwork. Recent studies [1]–[4] have conducted image vectorization by optimizing a fixed number of initialized parametric strokes, heavily relying on the use of differentiable rasterizers for loss backpropagation. As previously demonstrated, the reliance on pixel loss for backpropagation is suboptimal for vector graphics generation, often resulting in convergence to local optima or redundant predictions. Although these methods achieve visually appealing outcomes, they often neglect semantic information, leading to a tendency towards redundant shapes. Conversely, approaches such as [5], [6], which utilize Variational Autoencoders (VAEs) for SVG reconstruction, excel at preserving topological characteristics in vector generation. However, they failed to reach accurate shapes.

Different from representing image as a grid of pixels, SVG conceptualize images as sequences of parametric 2D shapes. These shapes comprise lists of lines or curves defined by specific points (or coordinates). Owing to its sequential and hierarchical nature, SVG can be simplified and represented as an extended sequence, enabling the application of recent advancements in Natural Language Processing (NLP), such as Recurrent Neural Networks (RNNs), Transformer-based models [7], Generative Pre-trained Transformer (GPT-2 [8]), and Multimodal NLP. Drawing inspiration from the hierarchical SVG generation pipeline utilized in DeepSVG [6], we introduce DeepIcon, a novel image vectorization network. DeepIcon is designed to hierarchically generate the final SVG from a single image input without depending on a differentiable rasterizer. Different from DeepSVG, we use a CLIP-based image encoder instead of a hierarchical SVG encoder. Also, we process the output SVG paths in the continuous space. Our experimental results demonstrate that DeepIcon outperforms state-of-the-art optimization-based vectorization approaches in preserving the topology similarity and geometric accuracy.

In summary, we have designed a novel hierarchical SVG generation model that converts an input RGB image into a high-quality SVG representation. Our contributions are three-

fold:

- As illustrated in Fig. 2, we developed an image vectorization pipeline named DeepIcon that facilitates high-quality image generation from images to Scalable Vector Graphics (SVG). This innovative pipeline not only achieves superior IMG-to-SVG translation fidelity but also ensures the preservation of the intrinsic geometric and relational information.
- We propose an accurate SVG decoder capable of generating a multi-path SVG result from a single embedding, denoted as z . Furthermore, we validate the versatility of the proposed decoder by demonstrating its applicability to various types of data inputs, provided that a corresponding encoder is available.
- We evaluate our method with a comparison to current state-of-the-art image vectorization and SVG generation approaches. The experimental results conclusively demonstrate that DeepIcon outperforms these methods both quantitatively and qualitatively.

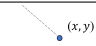
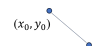
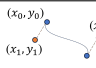
II. RELATED WORKS

A. Image Vectorization

Despite the straightforwardness of image rasterization from vectors, image vectorization from raster images is much more difficult due to the inadequate information provided in the image. Critical details such as the order of overlapping shapes, the direction in which a shape should be drawn, and the segmentation of shapes into distinct entities are not explicitly defined in raster images. While humans can often interpret these aspects intuitively, they pose considerable challenges for computational approaches, especially when dealing with complex images. In response to these challenges, learning-based approaches have been increasingly promising due to their efficiency in extracting higher-level information from images.

To bridge the gap between parametric attributes and image data, recent studies [1]–[4], [9], [10] adopt differentiable rasterizers to directly backpropagate pixel losses and optimize the parameters with consideration for the rasterized output, facilitating vector graphic generation without the need for ground-truth vector supervision. Moreover, Cloud2Curve [11] approaches the generation of parametric curves autoregressively from hand-drawn sketches by initially processing these

TABLE I: Description of SVG commands. By default, we set the start point for each path (a sequence of commands) as (0, 0). The default start point for each command is the end point of the last command in the path.

Command	Arguments	Description	Example
M (MoveTo)	x, y	Move the current cursor to point (x, y) .	
L (LineTo)	x, y	Draw a straight line from the current point (x_0, y_0) to point (x, y) .	
C (Cubic Bézier)	x_1, y_1 x_2, y_2 x, y	Draw a cubic bézier curve to point (x, y) with control points (x_1, y_1) and (x_2, y_2) .	

sketches into a sampled point cloud. Despite their innovative approach, reliance on differentiable rasterizers has shown its weakness of redundant shapes and convergence to local optima, underscoring a critical limitation in preserving topological integrity. An alternative approach conceptualizes vector graphics as executable graphics programs. Studies [12]–[17] have introduced their self-defined domain-specific language (DSL) that interprets vector graphics as compositions of various parametric primitives (e.g., circles, rectangles, straight lines and Lego bricks). There are also attempts such as [18]–[20] that incorporate additional knowledge (e.g., category, segmentation masks, and contours) to aid the vectorization process.

Unlike most existing vectorization approaches, our method does not rely on using a differentiable rasterizer or providing additional information. Operating solely with a single image input, DeepIcon can generate high-quality SVG representations featuring a variable number of shapes.

B. Vector Graphics Generation

Existing methods have proposed different vector representations with different aspects of simplifications. With the presentation of sketch datasets ‘Quick, Draw!’ [21], Sketch-RNN emerged as the first Sequence-to-Sequence Variational Autoencoder (VAE) model conducting conditional sketch generation and interpolation. Inspired by the success of Sketch-RNN, subsequent researchers proposed improved sketch generation approaches by leveraging the recent improvements in the Natural Language Processing (NLP) domain. For instance, Sketchformer [22] introduced a shift from LSTM to a Transformer-based architecture, achieving significant improvements in interpolation stability over Sketch-RNN. Similarly, [23], [24] focuses on the generation of stylized handwritten Chinese characters by disentangling style and content using two RNN-based or transformer-based encoders.

Sketches conceptualize vector graphics as a sequence of densely plotted points accompanied by corresponding pen states, which makes it flexible to represent a wide range of images. However, there is still a gap between such sketch representations and the widely adopted vector graphics formats (e.g., SVG). Some of the recent studies focus on generating complex vector graphics that incorporate both straight lines and curves, thereby introducing an inherent hierarchical structure to the sequential representation. Notably, [5], [25],

[26] proposed generative models specifically for SVG vector fonts, while [6] has concentrated on learning to generate SVG icons from a variational auto-encoder (VAE) based structure. Also, DeepSVG [6] makes an icon dataset public, providing the processed SVG annotations. [27] proposed methods for generating text-conditioned SVG icons using an autoregressive transformer, achieving high quality icon generation results.

Furthermore, there is also recent research focusing on the generation of graphics layouts. Similar to SVGs, graphics layouts are also composed of primitive types (e.g., topic categories and element types) and parametric arguments. [28]–[30] attempt conditional layout generation with different types of conditions provided (e.g., label sets, metadata, partial elements, and relation annotations). [31] learns to generate unconditional vector graphic documents through a transformer-based VAE structure.

Our proposed novel SVG generation network is inspired by DeepSVG [6], addressing the problem of poor geometric accuracy and improving the visual results by using autoregressive path decoders and predicting arguments in the continuous space.

III. DEEPICON

In this section, we first introduce the definition of our SVG representation (Section III-A) and the strategy for tokenization (Section III-B), followed by a comprehensive description to our proposed network (Section III-C). We then proceed to detail the implementation specifics of the training process (Section III-D).

A. SVG Representation

As a widely adopted representation, SVG offers a large range of commands and functionalities for designers to work with. To limit the scope for training and SVG inference, we simplified the representation of SVG by only picking the necessary attributes for icon representations. Here we present the SVG commands we choose to utilize in this paper as referenced in Table I. Since most basic shapes (e.g., rectangle, circle, ellipse, line, polyline and polygon) can be represented by a composition of straight lines and curves, with these three commands listed in the table, our model is capable of constructing a variety of shapes as through combinations of curves and lines. For instance, rather than employing the specialized *Rect* command for rectangles, we opt for a more fundamental

approach: initiating with the $M(x, y)$ command to move the cursor to a starting position, followed by the execution of four straight lines using the $L(x, y)$ command. By default, we set the initial point of each path at $(0, 0)$. Moreover, we simplify the command set by removing all attributes despite geometric arguments (coordinates of control points). Consequently, an SVG script S is succinctly represented as $S = \{P_i\}$, where P_i denotes the i^{th} path within the SVG script. Each path $P_i = \{C_i^j\}$ comprises a sequence of commands, where C_i^j denotes j^{th} command within P_i . N_P and N_C denote the number of paths and commands in each path respectively. Examples of the command implementations C_i^j are provided in Table I.

B. Tokenization

Different from most discrete tokenization methods, our approach to SVG decoding emphasizes enhanced geometric accuracy by treating point positions as continuous arguments. To facilitate this, we represent a single command implementation as $C_i^j = (\{T_k\}, \{A_k\})$ with a pair of sequences (with i and j omitted), where T_k and A_k denote the k^{th} elements of the type sequence T and argument sequence A , respectively. In detail, the $\{T_k\}$ sequence describes the discrete token types with $T_k \in \{M, L, C, \text{arg}, \text{SOS}, \text{EOS}\}$, while $\{A_k\}$ sequence indicates the continuous location arguments. These discrete tokens T_k respectively specify the token types MoveTo, LineTo, Cubic Bézier, continuous arguments, the start of SVG, and the end of SVG. Furthermore, to standardize the length of sequences for each command C_i^j , we also implement padding with a value of -1 for sequences T and A .

Sequences of commands within the same path P_i are then concatenated into a single pair of extended sequences for subsequent model processing. Consequently, the final tokenized representation of a path P_i is formulated as $P_i = (\{T_{j,k}\}, \{A_{j,k}\})$ (with i omitted), where $\{T_{j,k}\}$ and $\{A_{j,k}\}$ indicate the concatenated sequence of tokens for types and arguments within the i^{th} path, ensuring a coherent and standardized structure for autoregressive decoding. During training, the special tokens SOS and EOS are added to the start and end of type sequence $\{T_{j,k}\}$ respectively.

C. Model Architecture

We develop a hierarchical deep architecture, as illustrated in Fig. 3, designed to efficiently generate high-quality SVG scripts from a single input image. The illustrated model can be generally segmented into three principal modules: an image encoding module (CLIP Image Encoder), a structure decoding module (Transformer Decoder), and a path decoding module (Transformer Decoder). The input image is initially processed through the CLIP Image Encoder, augmented by a trainable Multi-layer Perceptron (MLP), to produce a singular image embedding, denoted as z_I . We adopt CLIP as the encoder to better capture the semantic information in the input image. Since the IMG-to-SVG task requires the model to bridge the image context with SVG scripts, which are written in an XML-based language, CLIP is well-suited due to its

strength in joint image-text embedding. Drawing inspiration from DeepSVG [6], this image embedding is subsequently input into a hierarchical SVG decoder, which operates in two distinct stages: 1) The structure decoder outputs a latent representation z_P and a corresponding visibility attribute v for each path P . Following this, the path decoder translates each path embedding z_P into a pair of tokens, as described in Section III-B.

1) *Structure Decoder*: The structure decoder within our architecture is comprised of a 4-layer Transformer decoder featuring a feed-forward dimension of 512 and a model dimension of 256. This transformer-based decoder is subsequently coupled with two trainable linear layers tasked with generating the path embeddings $z_P = (z_1, \dots, z_{N_P})$ and the visibility attributes $v = (v_1, \dots, v_{N_P})$ for each individual path P_i . Here $v_i \in \{0, 1\}$ serves as an indicator of path visibility. In this process, a predetermined number ($N_P = 8$ in this paper) of path and visibility pairs, denoted as $(z_{P,i}, v_i)$, are generated by iteratively feeding the image embedding z_I into the structure decoder. This innovative approach to predicting path visibility enables our network to generate SVG paths of variable lengths directly from the single image embedding, without the necessity for additional information.

2) *Path Decoder*: For the task of path decoding, we employ a 12-layer Transformer configured identically to the structure decoder. Each path decoder is also followed by 2 trainable linear layers designed to transform the output of the Transformer into two distinct sequences. The first sequence, a type sequence denoted as $\{T_{j,k}\}$, has a dimension of 6, corresponding to six different types of tokens. The second sequence, an argument sequence represented as $\{A_{j,k}\}$, contains continuous values. The continuous values $A_{j,k}$ in the argument sequence are only referenced when the predicted token $T_{j,k}$ in the type sequence is arg.

D. Training

Since we treat the SVG scripts as a pair of sequences, the primary training objective of our model is to minimize the three distinct loss components: the cross-entropy loss for types $\{T_{j,k}\}$, the cross-entropy loss for the path visibility attributes v_i and the mean squared error (MSE) for the valid arguments $\{A_{j,k}\}$. Therefore, for each path P_i , our objective is to optimize the model parameters Θ by minimizing the combined loss across these components:

$$\ell_i^{type} = \frac{1}{N} \sum CE(\hat{T}_{j,k}, T_{j,k} | I; \Theta), \quad (1)$$

$$\ell_i^{vis} = CE(\hat{v}_i, v_i | I; \Theta), \quad (2)$$

$$\ell_i^{args} = \frac{1}{N} \sum SE(\hat{A}_{j,k}, A_{j,k} | I; \Theta), \quad (3)$$

where N is the length of padded sequences for each path. $CE(\cdot, \cdot)$ denotes the cross-entropy function and $SE(\cdot, \cdot)$ refers to the squared error function, respectively. The symbol I represents the input image to the image vectorization model. The triplets $(T_{j,k}, \hat{A}_{j,k}, \hat{v}_i)$ and $(T_{j,k}, A_{j,k}, v_i)$ correspond

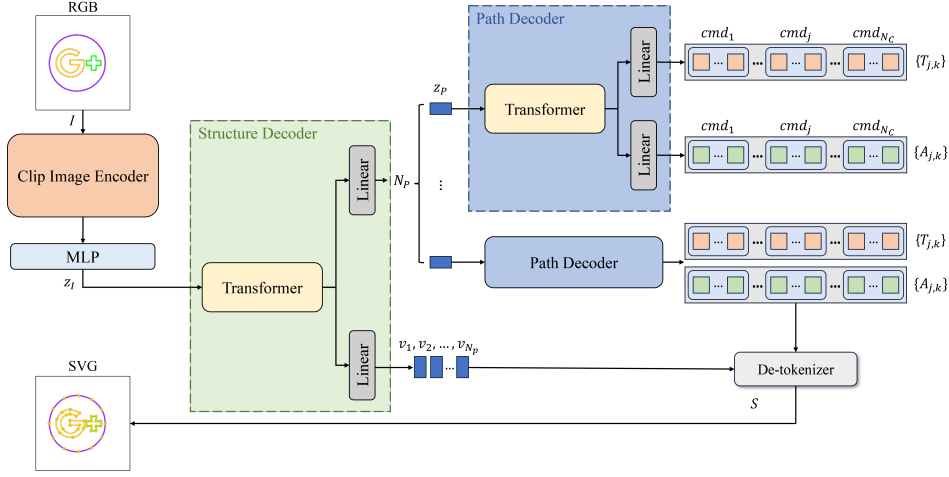


Fig. 3: The overall architecture of DeepIcon. The input image is encoded with a CLIP Image Encoder [32] to generate the latent embedding z_I . Then, it will be fed into a Structure Decoder to infer a series of path embeddings z_P and corresponding path visibility attributes v_P . For each path embedding, an individual path decoder outputs a pair of sequences $(\{T_{j,k}\}, \{A_{j,k}\})$ that defines the attributes and continuous arguments for each inferred SVG path. Here we use $T_{j,k}$ and $A_{j,k}$ to indicate the k^{th} tokens from the j^{th} command sequences within path P_i .

to the predicted and ground-truth attributes for each path P_i . Consequently, the final loss function for our model is constructed as a weighted sum of these 3 aforementioned losses, formalized as follows:

$$\ell(\hat{P}_i, P_i) = \omega_{vis} \ell_i^{vis} + v_i \cdot (\omega_{type} \ell_i^{type} + \omega_{args} \mathbf{1}_{T=\arg} \ell_i^{args}), \quad (4)$$

$$L(\hat{S}, S) = \sum_{i=1}^{N_P} \ell(\hat{P}_i, P_i), \quad (5)$$

where \hat{S} and S denote the predicted SVG scripts and the target SVG scripts respectively. The weights for ℓ^{vis} , ℓ^{type} and ℓ^{args} are denoted by ω_{vis} , ω_{type} , and ω_{args} . In this paper, we have assigned the values $\ell^{vis} = 1$, $\ell^{type} = 1$ and $\ell^{args} = 6 \times 10^3$ for training, effectively calibrating the emphasis on argument accuracy due to its critical role in ensuring geometric precision in the generated SVG paths.

1) *Decoder Pretraining*: We first pretrain the SVG decoders (i.e., the structure decoder and the path decoder) through an SVG-to-SVG reconstruction task, utilizing the SVG encoder module as designed by DeepSVG. The SVG coordinates are quantized to 8 bits and are individually embedded for input into the SVG encoder. Additionally, the types of commands are converted into embeddings of the same dimension using a learned matrix. The final input is thus a composite of the type embedding, argument embedding, and an additional learned index embedding. At this stage, the training objective is to minimize a loss function similar to that described in (5), without considering the input I :

$$L(\hat{S}, S|S, \Theta) = \sum_{i=1}^{N_P} \ell(\hat{P}_i, P_i). \quad (6)$$

2) *Joint Training*: Following the pretraining phase, we proceed to jointly finetune the CLIP image encoder and the

pretrained SVG decoders for an IMG-to-SVG generation task. This is achieved by integrating a trainable 3-layer Multilayer Perceptron (MLP) head to bridge the two components. Here we utilize a pretrained CLIP model with a ViT-L/14 Transformer architecture from the Hugging Face community. The loss function employed at this stage is consistent with that described in (5), thus can be written as:

$$L(\hat{S}, S|I, \Theta) = \sum_{i=1}^{N_P} \ell(\hat{P}_i, P_i). \quad (7)$$

IV. EXPERIMENTS AND RESULTS

In this section, we begin with an introduction to data preparation, as detailed in Section IV-A. Subsequently, we evaluate the performance of our proposed approach by conducting comparisons with state-of-the-art (SOTA) methods, as outlined in (Section IV-C), and by presenting ablation studies in Section IV-D.

A. Data Preprocessing

We evaluated our method using the publicly available SVG-Icons8 dataset, which was processed as described by [6]. This dataset includes a diverse collection of 100,000 SVG icons, categorized across 56 distinct classes. To tailor the dataset to our network's requirements, we implemented a filtering process to exclude icons that were deemed unsuitable for our experimental setup. Specifically, icons comprising more than 8 paths or those containing paths with more than 32 commands were excluded from consideration. Following this criterion, the refined dataset consisted of 25,990 SVG icons. These were subsequently divided into two distinct subsets for the purposes of training and evaluating respectively: 18,193 icons constituted the training set, and 7,797 icons were designated for evaluation. This partitioning was executed randomly to

TABLE II: Inference comparison results on the evaluation set.

Model	SVG-to-SVG		IMG-to-SVG	
	IoU (\uparrow)	CD (\downarrow)	IoU (\uparrow)	CD (\downarrow)
LIVE [1]	-	-	0.2513	-
DeepSVG [6]	0.3543	0.0257	0.2049	0.0399
DeepIcon (ours)	0.3730	0.0238	0.2203	0.0377

ensure a representative distribution of icon categories across both sets.

B. Implementation Details

We utilize the AdamW optimizer [33] for both pretraining and joint training processes. For decoder pretraining, we use the optimizer with an initial learning rate of 5×10^{-4} incorporating a linear warm-up over 500 steps. The pretraining phase lasts approximately 4 days, utilizing a batch size of 60 across 3 RTX 3090 GPUs. For joint training, we adopted a reduced learning rate of 10^{-6} and the model was trained over a span of approximately 4 days, with a batch size of 20.

C. Comparison with the State-of-the-art Methods

We compared the performance of our proposed model with two other leading state-of-the-art (SOTA) image vectorization and SVG generation methods: LIVE and DeepSVG. Given that DeepSVG’s primary application is the generation of SVG from the latent representations, we adapted it for direct comparison by finetuning the pretrained DeepSVG decoder in conjunction with the CLIP image encoder. The finetuning is employed in a similar procedure as that used for DeepIcon. The quantitative outcomes of this comparative analysis are presented in Table II. For the purposes of this quantitative comparison, we employed two evaluation metrics: Intersection over Union (IoU) and Chamfer Distance (CD), for their relevance and reliability in assessing the accuracy and quality of vector graphics.

1) *Quantitative Analysis*: Table II presents the quantitative results comparing our proposed model, DeepIcon, with SOTA vectorization methods, specifically LIVE and DeepSVG, across two distinct tasks: SVG-to-SVG reconstruction and IMG-to-SVG vectorization. The results indicate that DeepIcon outperforms DeepSVG in both tasks, demonstrating superior SVG generation accuracy. It is important to note that LIVE does not include a SVG encoder, thus becoming not applicable for the SVG-to-SVG reconstruction task. Therefore, this comparison is exclusively between DeepSVG and DeepIcon. In this task, DeepIcon exhibited higher average IoU and lower CD across the evaluation set, signaling more effective reconstruction performance with SVG data.

In the domain of IMG-to-SVG vectorization, DeepIcon maintains its superior performance over DeepSVG. When it comes to image vectorization, the SVG decoder of DeepIcon still performs better than DeepSVG. However, it is noteworthy that the IoU for DeepIcon is slightly lower than that of LIVE. This discrepancy can be attributed to LIVE’s approach of optimizing a stack of layered SVG paths through a differentiable

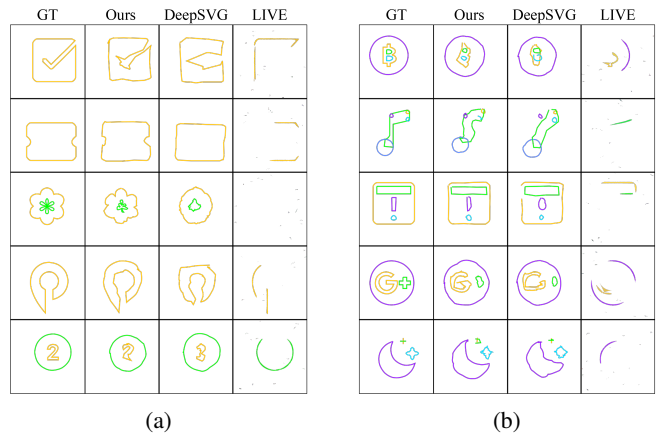


Fig. 4: Our qualitative comparison with SOTA methods DeepSVG and LIVE.

rasterizer, which inherently may offer advantages in specific contexts. As discussed in Fig. 1, methods that prioritize image fitting, such as LIVE, tend to achieve better results on pixel-based metrics.

2) *Qualitative Analysis*: Fig. 4 presents a qualitative comparison among DeepIcon, DeepSVG, and LIVE for the IMG-to-SVG task. It is evident that DeepIcon surpasses the other methods in preserving the structure of complex shapes, as illustrated in Fig. 4a. Furthermore, DeepIcon demonstrates a superior understanding of the relationships between overlapping shapes, enabling it to generate SVG paths with greater accuracy in terms of preserving the content semantics and relations between shapes. Although LIVE achieves the highest IoU as documented in Table II, it produces the least visually appealing results, as depicted in the figures. This outcome stems from the inherent limitations of parameter optimization methods, which, while adept at closely matching pixel values, often overlook higher-level information such as path relationships and the optimal number of paths. Consequently, LIVE tends to generate redundant but incomplete paths and is susceptible to falling into local optima.

D. Ablations

We conducted an ablation study on the evaluation set to validate the essential components of DeepIcon. By default, our configuration includes finetuning a pretrained decoder and a 3-layer MLP head, which is positioned after the CLIP image encoder to map the output embeddings to the input dimension required by the transformer. This study examines the impact of employing an autoregressive transformer, utilizing a continuous argument sequence, and applying finetuning techniques on the same dataset division. The outcomes of this investigation, including both quantitative and qualitative comparisons, are detailed in Table III and Fig. 5.

1) *Effectiveness of Autoregressive Transformer*: In our evaluation, we first analyze the impact of employing an autoregressive transformer compared to a non-autoregressive approach in the path decoder’s design. The non-autoregressive decoder

TABLE III: Quantitative results of ablation study over the IMG-to-SVG generation task. The ‘Finetune’ column denotes whether or not to finetune the pretrained CLIP image encoder. Additionally, we explore the implementation of a non-autoregressive decoder, which is based on the design principles outlined by [6]. Detailed explanations of these design choices and their implications are provided in Section IV-D.

Model	Finetune	Decoder	Args	IoU (\uparrow)	CD (\downarrow)
A	✓	Non-autoregressive	Discrete	0.2049	0.0399
B	✗	Autoregressive	Discrete	0.0669	0.1110
C	✓	Autoregressive	Discrete	0.1868	0.0442
D	✗	Autoregressive	Continuous	0.0818	0.0951
E	✓	Autoregressive	Continuous	0.2203	0.0377

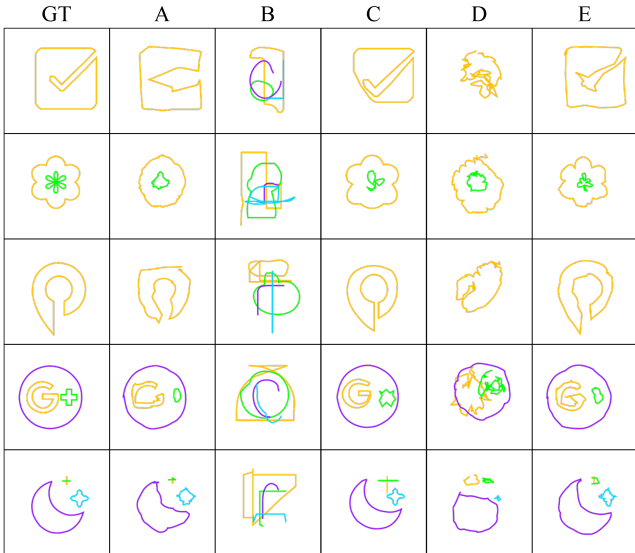


Fig. 5: Ablation study on our proposed image vectorization network. The first column showcases the target image, which also serves as the input for our models. The specific configurations for models A through E are detailed in Table III.

projects the transformer’s output dimension directly to the product of the number of arguments in a command and the argument embedding dimension, denoted as $n_{args} \times d_{args}$, where $n_{args} = 11$. Unused arguments within the command sequence are padded with -1 . Consequently, the non-autoregressive decoder processes path embeddings as inputs and predicts tokens by the unit of commands. As demonstrated in Model A and C of Table III and Fig. 5, employing a non-autoregressive transformer decoder leads to a noticeable decline in accuracy, as evidenced by the lower IoU and higher CD . However, autoregressive decoder provides apparently better visual performance, yielding much clearer shapes delineations and superior semantics consistency. This suggests that while autoregressive decoders are adept at capturing and reproducing the semantic essence of shapes, they struggle with precise geometric positioning.

2) *Effectiveness of Continuous Arguments*: Then, we examine the impact of transitioning arguments into a continuous space for prediction. The details of the implementation

are introduced in Section III-B. Given the observed trade-offs between autoregressive and non-autoregressive decoding approaches, our goal is to preserve the semantic understanding benefits offered by the autoregressive transformer while addressing its limitations in terms of coordinate inference accuracy. By shifting to a continuous space, we observe significant improvements, both quantitatively and qualitatively. Predicting arguments in the continuous space not only enhances the accuracy of coordinate predictions but also maintains the autoregressive transformer’s advantage in capturing the semantics of shapes.

3) *Effectiveness of Finetuning*: While most downstream applications employ the CLIP image encoder as a zero-shot encoder with an additional MLP (Multilayer Perceptron) head for training, we compare the outcomes with and without finetuning the CLIP image encoder, as depicted in Table III and Fig. 5. Without finetuning, the discrete space SVG (Scalable Vector Graphics) decoder struggles to learn effectively from the examples, resulting in relatively random SVG outputs, as illustrated in the column B of Fig. 5. This issue is partially addressed by adopting continuous arguments, as demonstrated in the column D of Fig. 5. However, the results still fall short of those achieved with a finetuned CLIP encoder.

V. CONCLUSION

This paper introduces a novel image vectorization network designed to generate variable-length SVG scripts from a single image input, reconstructing its structure with an emphasis on semantic consistency. DeepIcon reconceptualizes SVG icon representation as a sequence of paths, wherein each path consists of a variable number of commands delineating parametric lines or curves, thereby prioritizing the completion of topological structures. The model is trained and evaluated on the SVG-Icons8 dataset. Utilizing the CLIP image encoder and the hierarchical transformer-based SVG decoder, our network effectively bridges the gap between images and SVG scripts. The introduction of a unique tokenization rule and the alignment of continuous arguments further enhance the model’s performance. The quantitative and qualitative results from our experiments demonstrate that DeepIcon surpasses state-of-the-art approaches, achieving high-quality icon vectorization results.

Limitation. While the DeepIcon model demonstrates achievements in the domain of icon vectorization, it remains

improvable. While the reconstruction accuracy of the icon vectorization process is not yet perfect, it suggests an opportunity for the development of a more sophisticated SVG decoder, aimed at significantly enhance SVG decoding performance. Also, DeepIcon is limited to predicting relatively simple SVG shapes, with a maximum of 8 paths and no more than 32 commands per path.

Future Works. Enhancing the capabilities of the SVG decoder could not only improve the model’s accuracy but also reduce its reliance on the finetuning of the CLIP image encoder. Such advancements could pave the way for the model’s extension into new applications, including text-to-SVG generation. By potentially substituting the image encoder with a pretrained CLIP text model, DeepIcon could be adapted to interpret and translate textual descriptions into SVG scripts, broadening its applicability and utility in the field of graphic representation.

REFERENCES

- [1] X. Ma, Y. Zhou, X. Xu, B. Sun, V. Filev, N. Orlov, Y. Fu, and H. Shi, “Towards layer-wise image vectorization,” *IEEE/CVF Conference on Computer Vision and Pattern Recognition*, 2022.
- [2] T. Li, M. Lukác, M. Gharbi, and J. Ragan-Kelley, “Differentiable vector graphics rasterization for editing and learning,” *ACM Transactions on Graphics*, vol. 39, pp. 1–15, 2020.
- [3] S. Liu, T. Lin, D. He, F. Li, R. Deng, X. Li, E. Ding, and H. Wang, “Paint transformer: Feed forward neural painting with stroke prediction,” *IEEE/CVF International Conference on Computer Vision*, pp. 6578–6587, 2021.
- [4] Z. Zou, T. Shi, S. Qiu, Y. Yuan, and Z. Shi, “Stylized neural painting,” *IEEE/CVF Conference on Computer Vision and Pattern Recognition*, pp. 15 684–15 693, 2020.
- [5] R. G. Lopes, D. R. Ha, D. Eck, and J. Shlens, “A learned representation for scalable vector graphics,” *IEEE/CVF International Conference on Computer Vision*, pp. 7929–7938, 2019.
- [6] A. Carlier, M. Danelljan, A. Alahi, and R. Timofte, “Deepsvg: A hierarchical generative network for vector graphics animation,” *Advances in Neural Information Processing Systems*, vol. 33, pp. 16 351–16 361, 2020.
- [7] A. Vaswani, N. Shazeer, N. Parmar, J. Uszkoreit, L. Jones, A. N. Gomez, L. u. Kaiser, and I. Polosukhin, “Attention is all you need,” in *Advances in Neural Information Processing Systems*, vol. 30, 2017.
- [8] T. Brown, B. Mann, N. Ryder, M. Subbiah, J. D. Kaplan, P. Dhariwal, A. Neelakantan, P. Shyam, G. Sastry, A. Askell, S. Agarwal, A. Herbert-Voss, G. Krueger, T. Henighan, R. Child, A. Ramesh, D. Ziegler, J. Wu, C. Winter, C. Hesse, M. Chen, E. Sigler, M. Litwin, S. Gray, B. Chess, J. Clark, C. Berner, S. McCandlish, A. Radford, I. Sutskever, and D. Amodei, “Language models are few-shot learners,” in *Advances in Neural Information Processing Systems*, vol. 33, 2020, pp. 1877–1901.
- [9] Y. Vinker, E. Pajouheshgar, J. Y. Bo, R. C. Bachmann, A. H. Bermanno, D. Cohen-Or, A. Zamir, and A. Shamir, “Clipasso: semantically-aware object sketching,” *ACM Transactions on Graphics*, vol. 41, 2022.
- [10] H. Lee, I. Hwang, H. Go, W. Choi, K. Kim, and B. Zhang, “Learning geometry-aware representations by sketching,” in *IEEE/CVF Conference on Computer Vision and Pattern Recognition*, 2023, pp. 23 315–23 326.
- [11] A. Das, Y. Yang, T. M. Hospedales, T. Xiang, and Y.-Z. Song, “Cloud2curve: Generation and vectorization of parametric sketches,” *IEEE/CVF Conference on Computer Vision and Pattern Recognition*, pp. 7084–7093, 2021.
- [12] K. Ellis, M. Nye, Y. Pu, F. Sosa, J. Tenenbaum, and A. Solar-Lezama, “Write, execute, assess: Program synthesis with a repl,” in *Advances in Neural Information Processing Systems*, vol. 32, 2019.
- [13] G. Sharma, R. Goyal, D. Liu, E. Kalogerakis, and S. Maji, “Csgnet: Neural shape parser for constructive solid geometry,” *IEEE/CVF Conference on Computer Vision and Pattern Recognition*, 2018.
- [14] J. Feser, I. Dillig, and A. Solar-Lezama, “Inductive program synthesis guided by observational program similarity,” *Proceedings of the ACM on Programming Languages*, vol. 7, pp. 912–940, 2023.
- [15] S. Dumancic, T. Guns, and A. Cropper, “Knowledge refactoring for inductive program synthesis,” *Proceedings of the AAAI Conference on Artificial Intelligence*, vol. 35, pp. 7271–7278, 2021.
- [16] K. Ellis, D. Ritchie, A. Solar-Lezama, and J. Tenenbaum, “Learning to infer graphics programs from hand-drawn images,” in *Advances in Neural Information Processing Systems*, vol. 31, 2018.
- [17] Q. Bing, C. Zhang, and W. Cai, “Learning to synthesize graphics programs for geometric artworks,” in *The International Conference on Pattern Recognition*, 2024.
- [18] I. Shen and B. Chen, “Clipgen: A deep generative model for clipart vectorization and synthesis,” *IEEE Transactions on Visualization and Computer Graphics*, vol. 28, pp. 4211–4224, 2021.
- [19] H. Zhu, J. I. Chong, T. Hu, R. Yi, Y.-K. Lai, and P. L. Rosin, “Samvg: A multi-stage image vectorization model with the segment-anything model,” *IEEE International Conference on Acoustics, Speech and Signal Processing*, 2024.
- [20] Y.-T. Liu, Z. Zhang, Y.-C. Guo, M. Fisher, Z. Wang, and S.-H. Zhang, “Dualvector: Unsupervised vector font synthesis with dual-part representation,” in *IEEE/CVF Conference on Computer Vision and Pattern Recognition*, 2023, pp. 14 193–14 202.
- [21] D. Ha and D. Eck, “A neural representation of sketch drawings,” in *International Conference on Learning Representations*, 2018.
- [22] L. Sampaio Ferraz Ribeiro, T. Bui, J. Collomosse, and M. Ponti, “Sketchformer: Transformer-based representation for sketched structure,” in *IEEE/CVF Conference on Computer Vision and Pattern Recognition*, 2020, pp. 14 141–14 150.
- [23] S. Tang and Z. Lian, “Write like you: Synthesizing your cursive online chinese handwriting via metric-based meta learning,” in *Computer Graphics Forum*, vol. 40, no. 2, 2021, pp. 141–151.
- [24] G. Dai, Y. Zhang, Q. Wang, Q. Du, Z. L. Yu, Z. Liu, and S. Huang, “Disentangling writer and character styles for handwriting generation,” *IEEE/CVF Conference on Computer Vision and Pattern Recognition*, pp. 5977–5986, 2023.
- [25] H. Aoki and K. Aizawa, “Svg vector font generation for chinese characters with transformer,” *IEEE International Conference on Image Processing*, pp. 646–650, 2022.
- [26] D. Cao, Z. Wang, J. Echevarria, and Y. Liu, “Svgformer: Representation learning for continuous vector graphics using transformers,” in *IEEE/CVF Conference on Computer Vision and Pattern Recognition*, 2023, pp. 10 093–10 102.
- [27] R. Wu, W. Su, K. Ma, and J. Liao, “Iconshop: Text-guided vector icon synthesis with autoregressive transformers,” *ACM Transactions on Graphics*, vol. 42, pp. 1 – 14, 2023.
- [28] A. Jyothi, T. Durand, J. He, L. Sigal, and G. Mori, “Layoutvae: Stochastic scene layout generation from a label set,” in *IEEE/CVF International Conference on Computer Vision*, 2019, pp. 9894–9903.
- [29] X. Zheng, X. Qiao, Y. Cao, and R. W. H. Lau, “Content-aware generative modeling of graphic design layouts,” *ACM Transactions on Graphics*, vol. 38, pp. 1 – 15, 2019.
- [30] H.-Y. Lee, W. Yang, L. Jiang, M. Le, I. Essa, H. Gong, and M.-H. Yang, “Neural design network: Graphic layout generation with constraints,” *Proceedings of the European Conference on Computer Vision*, pp. 491–506, 2020.
- [31] K. Yamaguchi, “Canvasvae: Learning to generate vector graphic documents,” *IEEE/CVF International Conference on Computer Vision*, pp. 5461–5469, 2021.
- [32] A. Radford, J. W. Kim, C. Hallacy, A. Ramesh, G. Goh, S. Agarwal, G. Sastry, A. Askell, P. Mishkin, J. Clark, G. Krueger, and I. Sutskever, “Learning transferable visual models from natural language supervision,” in *Proceedings of the 38th International Conference on Machine Learning*, vol. 139, 2021, pp. 8748–8763.
- [33] I. Loshchilov and F. Hutter, “Decoupled weight decay regularization,” in *International Conference on Learning Representations*, 2019.